

Chemical Transport and Electronic Properties of Europium Compounds with Complex Anions

Sylvia Golbs, Raul Cardoso-Gil, Alim Ormezi, Rainer Pöttgen¹, Falko Schappacher¹, Marcus Schmidt, Walter Schnelle, and Yuri Grin

The focus of our recent studies was based on chemical transport behavior, crystal growth, crystal structure, thermodynamic description and simulation on rare-earth metal compounds with complex anions [1,2]. We paid special attention to the chemical transport of EuPnO_4 ($Pn = \text{P, As, Sb}$) and the investigation of their physical properties depending on the participating complex anion.

Within the row P-As-Sb the stability of the oxidation state +5 decreases continuously. Thus, pentavalent antimony compounds are less stable at higher temperatures than their lower homologues. There is also a recognizable trend in the electronegativity. According to *Mulliken* ($\text{EN}_\text{P} = 2.4$, $\text{EN}_\text{As} = 2.3$ and $\text{EN}_\text{Sb} = 2.1$) [3] and *Pauling* ($\text{EN}_\text{P} = 2.2$, $\text{EN}_\text{As} = 2.2$ and $\text{EN}_\text{Sb} = 2.1$) [4] the electronegativity decreases in the row P-As-Sb. It is known that the EuPnO_4 compounds crystallize in three different structure types. EuPO_4 possesses the monoclinic monazite-type crystal structure (space group $P2_1/n$) [5], EuAsO_4 forms the tetragonal xenotime-type structure (space group $I4_1/amd$) [6]. The crystal structure of EuSbO_4 was determined and refined in the space group $P2_1/c$ [2]. An important difference between these structures is the spatial isolation of $[\text{PO}_4]^{3-}$ and $[\text{AsO}_4]^{3-}$ tetrahedra, whereas the $[\text{Sb}_2\text{O}_2\text{O}_{4/2}]^{3-}$ octahedra are chain-connected along b and c .

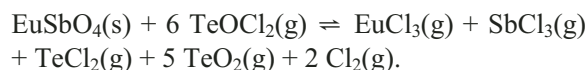
The transport experiments were carried out in evacuated quartz glass tubes, starting from microcrystalline powder materials. Single crystals of EuPO_4 were grown by chemical vapor transport with PCl_5 as transport agent in the temperature range of $T_2 = 1353 \text{ K}$ to $T_1 = 1253 \text{ K}$ [7]. EuAsO_4 crystals were grown by endothermic chemical transport reaction with a temperature gradient $T_2 = 1353 \text{ K}$ to $T_1 = 1243 \text{ K}$ using TeCl_4 as transport agent [1]. Crystals of EuSbO_4 were obtained by an endothermic transport reaction from 1373 K to 1223 K with TeCl_4 as transport agent [2]. It was observed that the transport rate and crystal size decreases from the phosphate(V) to the antimonate(V). This fact is associated with the strong

corrosion of the quartz glass tube, which increases significantly from the phosphate(V) to the antimonate(V).

For thermodynamic description as well as model calculations, simulations and prediction of optimal transport conditions, it is necessary to know all condensed phases and all gaseous species present in the systems and their thermodynamic characteristics. The program package TRAGMIN 5 [8] was used to describe the solid-phase/gaseous-phase equilibrium, the composition of the gaseous phase, as well as the temperature-dependent partial pressure curve and the transport efficiency of various species.

The calculations were performed for the chemical transport reactions of EuPO_4 with PCl_5 and EuSbO_4 with TeCl_4 . The temperature gradient was equally chosen to that used in the experiment. The following solid phases were taken into account for both systems: Eu_2O_3 , EuOCl and EuCl_3 . Additionally, the specific compounds EuPO_4 and P_4O_{10} for the system $\text{EuPO}_4/\text{PCl}_5$ as well as EuSbO_4 , SbOCl , SbCl_3 , Sb_2O_3 , Sb_2O_4 and Sb_2O_5 for the system $\text{EuSbO}_4/\text{TeCl}_4$ were considered. The species of the gaseous phase were determined with Knudsen cell mass spectrometry. Figure 1 shows the calculated composition of the gaseous phase of a EuPO_4 source, which is in equilibrium with PCl_5 in the temperature range from 1253 K to 1353 K . The dominating gaseous species are $\text{POCl}_3(\text{g})$, $\text{EuCl}_3(\text{g})$, $\text{PCl}_3(\text{g})$ and $\text{Cl}_2(\text{g})$. $\text{PCl}_3(\text{g})$ and $\text{Cl}_2(\text{g})$ were formed through the thermal decomposition of PCl_5 . The partial pressures of $\text{PO}_2(\text{g})$ ($10^{-7.5} \text{ bar}$), $\text{PO}(\text{g})$ ($10^{-8.5} \text{ bar}$) and $\text{O}_2(\text{g})$ (10^{-10} bar) are smaller than 10^{-5} bar , which implies that these species do not have significant transport effects. By means of the calculated transport efficiency, the endothermic transport behaviour was described. The transport reaction of EuPO_4 takes place by consuming $\text{POCl}_3(\text{g})$ and formation of $\text{POCl}(\text{g})$, $\text{Cl}_2(\text{g})$ and $\text{EuCl}_3(\text{g})$, whereas $\text{EuCl}_3(\text{g})$ is the europium-transporting species and phosphorous is basically transported by $\text{POCl}(\text{g})$.

The calculated gaseous phase composition of the system $\text{EuSbO}_4/\text{TeCl}_4$ in the temperature range from 1223 K to 1373 K is presented in Fig. 2. $\text{TeOCl}_2(\text{g})$ and $\text{SbCl}_3(\text{g})$ are the dominating species in the gaseous phase. Due to the decomposition of the transport agent TeCl_4 the partial pressure of $\text{TeCl}_2(\text{g})$ and $\text{Cl}_2(\text{g})$ is also relatively high. The partial pressure of the europium-containing species $\text{EuCl}_3(\text{g})$ of around 10^{-5} bar is just at the border of transport-efficiency. Thus, europium is transported by $\text{EuCl}_3(\text{g})$, but with a much lower rate as in the case of EuPO_4 . Furthermore, $\text{SbCl}_3(\text{g})$ should be the antimony-transporting species. The transport efficiency of $\text{EuCl}_3(\text{g})$ ($\Delta[p_i/p_L] = 0.00171$) and $\text{SbCl}_3(\text{g})$ ($\Delta[p_i/p_L] = 0.00173$) are, as expected, nearly the same. $\text{Te}(\text{g})$, $\text{Te}_2(\text{g})$, $\text{EuCl}_2(\text{g})$ and $\text{SbOCl}(\text{g})$ with partial pressures lower than 10^{-5} bar do not influence the transport reaction. With the results of the calculated efficiency the observed endothermic transport behavior of EuSbO_4 was described by the following equilibrium:



This equation shows that the real transport agent is $\text{TeOCl}_2(\text{g})$ and not, as presumed, TeCl_4 . $\text{TeOCl}_2(\text{g})$ is formed by the simultaneous reaction:

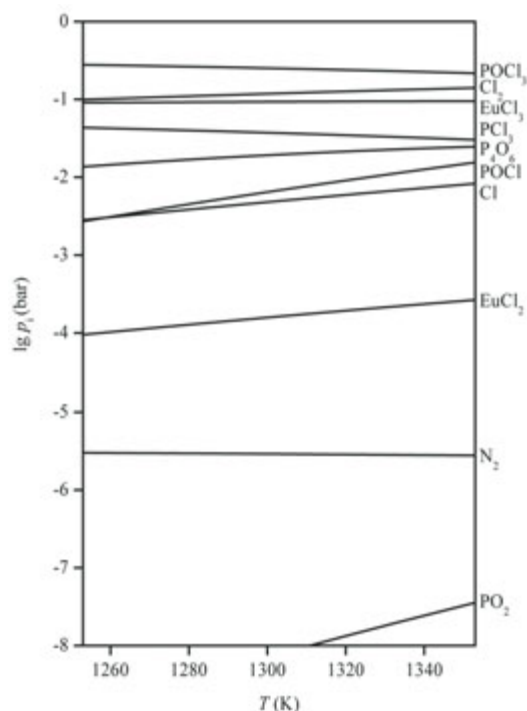
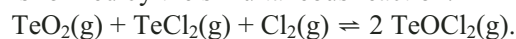


Fig. 1: Gaseous phase composition of EuPO_4 with PCl_5 .

The system $\text{EuAsO}_4/\text{TeCl}_4$ is similar to the antimony system. The only difference in the case of EuAsO_4 is that $\text{AsCl}_3(\text{g})$ appears as the arsenic transporting species.

The valence state of europium in the ternary compounds EuPnO_4 ($Pn = \text{P, As, Sb}$) was determined using X-ray absorption near edge spectroscopy (XANES) at the $\text{Eu } L_{\text{III}}$ threshold. Eu_2O_3 was used as standard for energy calibration and to determine the shift of the $\text{Eu } L_{\text{III}}$ edge of each compound. Figure 3 shows the normalized spectra of EuPnO_4 ($Pn = \text{P, As, Sb}$) in comparison to the trivalent reference compound Eu_2O_3 . All spectra are identified by a maximum of the absorption edge at 6993(1) eV and the well-known single ‘white line’ structure, characteristic for europium in the $4f^6$ configuration (Eu^{3+}).

The reliable determination of the specific heat posed a problem due to the small crystal sizes. Results obtained on samples of selected crystals with a total mass of ≈ 10 mg for each compound are given in Fig. 4. While the standard values of specific heat, entropy and enthalpy at 298.15 K are similar for EuAsO_4 ($S^\circ = 128.9(1.3) \text{ J mol}^{-1} \text{ K}^{-1}$) and EuSbO_4 ($S^\circ = 126.5(1.3) \text{ J mol}^{-1} \text{ K}^{-1}$), the corresponding values for EuPO_4 ($S^\circ = 113.7(1.1) \text{ J mol}^{-1} \text{ K}^{-1}$) are lower.

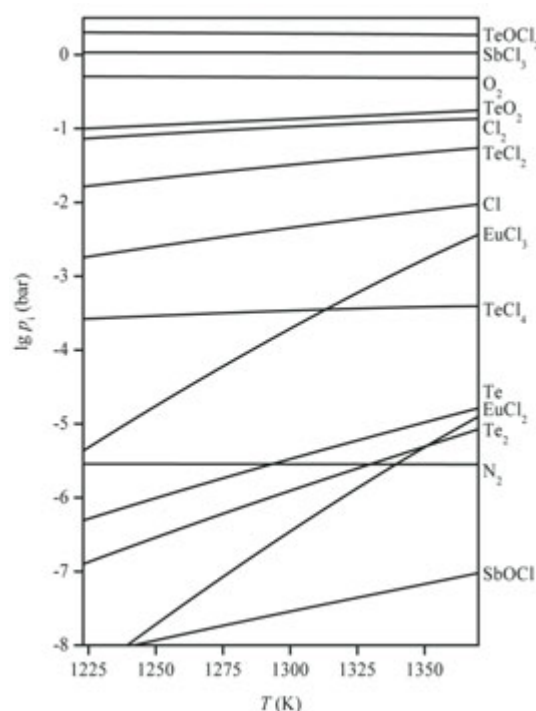


Fig. 2: Gaseous phase composition of EuSbO_4 with TeCl_4 .

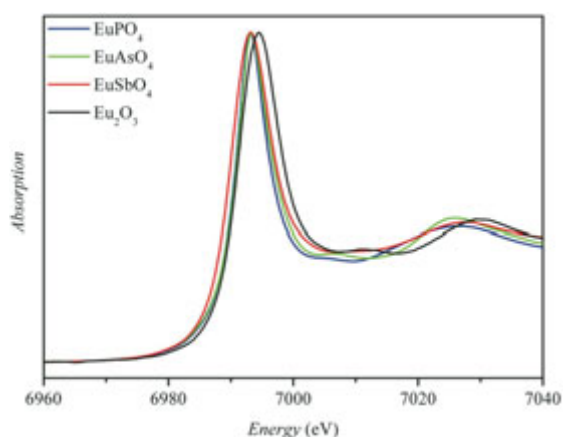


Fig. 3: XAS spectra of EuPnO_4 ($Pn = P, As, Sb$) at the Eu L_{III} edge.

Differences in the elastic properties of the compounds are visible in the specific heat at low temperatures (Fig. 4. inset). While for the two higher homologues the Debye T^3 law holds to ≈ 20 K, deviations become visible already above 10 K for EuPO_4 , indicating a more heterogeneous bonding situation for this structure. The low Debye temperature Θ_D (EuPO_4 : 495 K; cf. EuAsO_4 : 371 K and EuSbO_4 : 359 K) of EuPO_4 indicates a generally rigid framework. No linear term or magnetic contributions are visible in the specific heat, in agreement with the fact that all three compounds are insulators with non-magnetic ground state. Temperature dependence of the magnetic susceptibility reflects the non-magnetic 7F_0 crystal field ground state and excited 7F_n ($n = 1-6$) states of the $4f^6$ configuration of Eu^{3+} in good agreement with the XANES results. The susceptibilities at 0 K are finite due to the Zeeman coupling of the ground state with the (first) excited level and largest for EuSbO_4 . The excess specific heat of EuAsO_4 compared to EuSbO_4 in the range 80 K – 180 K (Fig. 4) might be partially due to a Schottky anomaly resulting from a different energy splitting of the excited 7F_n levels in the two compounds. This variation in spin-orbit coupling of Eu may be caused by different coordination of Eu in these compounds.

The ${}^{151}\text{Eu}$ Mössbauer spectra of EuPnO_4 ($Pn = P, As, Sb$) at 77 K are presented in Fig. 5 together with transmission integral fits. All three compounds show single europium signals subject to weak quadrupole splitting, in agreement with the

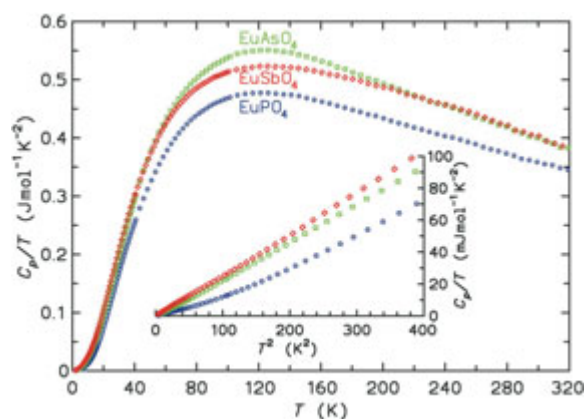


Fig. 4: Molar heat capacity C_p/T for EuPnO_4 compounds. The inset shows the low-temperature data in a C_p/T vs. T^2 representation.

crystal structures. The isomer shifts are around 0 mm/s as expected for trivalent europium. From the phosphate(V) to the antimonate(V) the isomer shifts vary from 0.16 to 0.86 mm/s, reflecting the different electronegativities of phosphorous, arsenic and antimony. The change in electro-negativity of the p element influences the electron density at the europium nuclei. A similar behavior is observed in the series

EuF_3 (−0.59 mm/s) \rightarrow EuCl_3 (−0.42 mm/s) \rightarrow EuBr_3 (−0.06 mm/s) and EuOF (−0.72 mm/s) \rightarrow EuOCl (−0.43 mm/s) \rightarrow EuOBr (−0.29 mm/s) \rightarrow EuOI (+0.02 mm/s) [9].

Thus the highest electron density is observed at the europium nuclei of EuSbO_4 . The experimental line width shows the usual values for europium.

The electronic structures of the three compounds are investigated by a full-potential local orbital method (FPLO [10]). The calculations carried out within the local spin density approximation (LSDA) yield metallic density of states (DOS), in clear contradiction to the experimental evidence. Therefore, the strong correlations among the Eu $4f$ electrons have to be taken into account via the LSDA+ U approach, using $U = 8$ eV in the calculations. The DOS obtained for an antiferromagnetic (AFM) arrangement of Eu magnetic moments are shown in Fig. 6. Wide energy gaps are found for each compound, in good agreement with experimental indications. Topo-logical analysis of electron localizability indicator (ELI) shows that mainly ionic bonding is operative in this group of compounds.

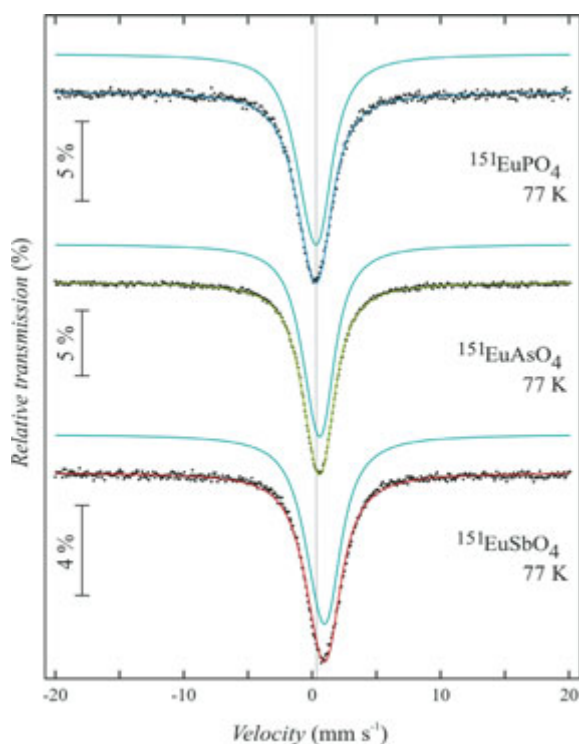


Fig. 5: Experimental and simulated ^{151}Eu Mössbauer spectra of EuPnO_4 ($\text{Pn} = \text{P}, \text{As}, \text{Sb}$) at 77 K.

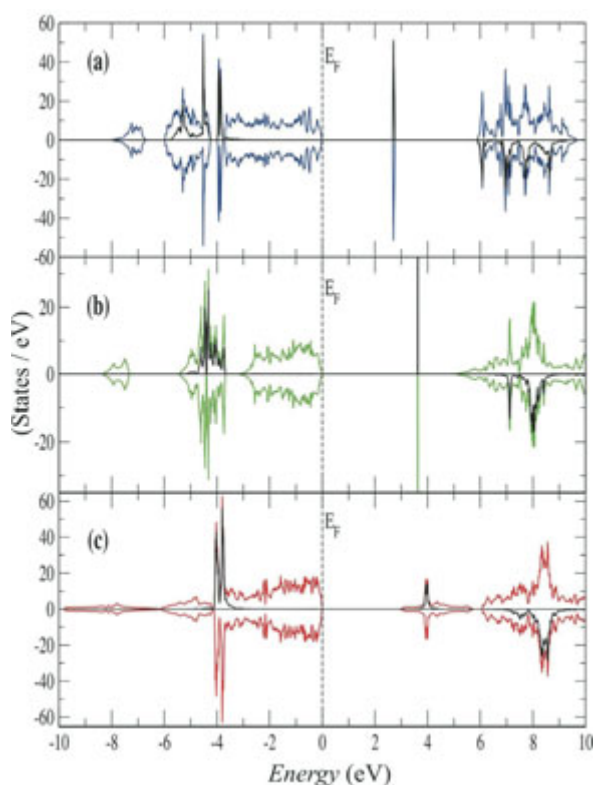


Fig. 6: The total (black lines) and Eu 4f DOS computed for EuPO_4 (a), EuAsO_4 (b) and EuSbO_4 (c). LSDA+U approach is used with $U = 8$ eV. Eu spin magnetic moments are coupled antiferromagnetically.

Conclusion

The experimental results of the XAS and Mössbauer spectroscopy as well as the band gaps, calculated from the density of states, show that the electronegativity of the complex anion decreases in the series from the phosphate and the arsenate to the antimonate. Thereby, the difference between EuPO_4 and EuAsO_4 is obviously smaller than between EuAsO_4 and EuSbO_4 . This is in agreement with the trend of the electronegativity of the elements P, As and Sb.

References

- [1] M. Schmidt, U. Müller, R. Cardoso-Gil, E. Milke, and M. Binnewies, *Z. Anorg. Allg. Chem.* **631** (2005) 1154.
- [2] S. Gerlach, R. Cardoso-Gil, E. Milke, and M. Schmidt, *Z. Anorg. Allg. Chem.* **633** (2007) 83.
- [3] R. S. Mulliken, *J. Chem. Phys.* **2** (1934) 782.
- [4] L. Pauling, *The Nature of the Chemical Bond*, 3rd ed, Cornell University Press, Ithaca, NY, 1960.
- [5] D. F. Mullica, and D. A. Grossie, *Inorg. Chim. Acta* **109** (1985) 105.
- [6] S. Golbs, R. Cardoso-Gil, and M. Schmidt, NCS, in preparation
- [7] V. P. Orlovskii, H. Schäfer, V. P. Repko, G. M. Safronov, and I. V. Tananaev, *Neorg. Mater.* **7** (1971) 971.
- [8] G. Krabbes, W. Bieger, K.-H. Sommer, T. Söhnel, and U. Steiner, TRAGMIN Version 5.0, Dresden 2007.
- [9] J. G. Stevens, V. E. Stevens, P. T. Deason Jr., A. H. Muir, H. M. Coogan and R. W. Grant, *Mössbauer Effect Data Index*, IFI/Plenum Data Company, New York, 1975.
- [10] K. Koepf and H. Eschrig, *Phys. Rev. B* **59** (1999) 1743.

¹ Westfälische Wilhelms-Universität Münster, Münster, Germany